Conference on Modelling Fluid Flow (CMFF'25)
The 19th International Conference on Fluid Flow Technologies
Budapest, Hungary, August 26 - August 29, 2025

SIMULATION AND CHALLENGES FOR A LOW SPECIFIC SPEED PELTON TURBINE

Daniel R. REITERER[1], Lukas SANDMAIER[2], Helmut BENIGNI[3]

[1] Corresponding Author. Institute of Hydraulic Fluid Machinery, Graz University of Technology. E-mail: daniel.reiterer@gmx.net
[2] Institute of Hydraulic Fluid Machinery, Graz University of Technology. E-mail: lukas.sandmaier@tugraz.at
[3] Institute of Hydraulic Fluid Machinery, Graz University of Technology. E-mail: helmut.benigni@tugraz.at

ABSTRACT

This study presents the numerical analysis of a Pelton turbine of low specific speed with the Lagrangian open-source code DualSPHysics [1]. The numerical results were compared with experimental data. The main objective was to determine if the applied numerical approach led to reproducible results and allowed insight into the momentum transfer and water movement in jet, runner, and casing. The influence of numerical parameters like particle size, kernel and smoothing length coefficient, and shifting value on the simulation results has been tested.

As a result, an optimal particle size formulation is suggested. Furthermore, we established a connection for two numerical parameters of DualSPHysics, the "smoothing length coefficient" and the "shifting", to improve the fluid flow behaviour and the resulting torque without modifying the physical parameters. In addition, we investigated the deviation from the optimal achievable torque and the improved fluid behaviour through these numerical parameters.

We discussed the effect of the bucket disturbance in the jet from the particle simulation alongside the similarity law simulation and the actual prototype's measurement outcomes. Identical simulations of the physical properties of the operation points were compared in momentum.

Keywords: Pelton turbine, SPH, DualSPHysics, Particle simulation

NOMENCLATURE

A	$[m^2]$	cross-section
B	$[m]$	bucket width
$coef_h$	[-]	kernel smoothing coefficient
D	$[m]$	runner jet diameter
d_{jet}	$[m]$	diameter of the jet
d_p	$[m]$	particle size
g	$[m^2/s]$	gravitational constant
H	$[m]$	head
k_c	[-]	nozzle losses
k_{dp}	[-]	jet diameter/particle coefficient
k_{jv}	[-]	kinetic energy coefficient
kh	[-]	smoothing length
n	$[1/s]$	rotational runner speed
Q	$[m^3/s]$	discharge
T	$[Nm]$	torque
t	$[s]$	time
TFS	[-]	threshold to detect free surface
v	$[m/s]$	velocity vector
z	[-]	number of buckets
φ	[-]	discharge coefficient
ψ	[-]	pressure coefficient

Subscripts and Superscripts

jet	fluid jet of a single nozzle
M	meridional speed
x, y, s	cartesian coordinate components
I	low specific speed prototype
II,	typical specific speed prototypes
PS, SS	pressure side, suction side

1. INTRODUCTION

Pelton turbines with a low specific speed n_q operate with comparatively low flow rates and high heads. This type of Pelton turbine is often used in systems whose purpose is not primarily power generation, such as in water supply or process engineering systems. Therefore, such turbines' design, analysis, and optimisation are often restricted by low budgets and require cost-effective methods. In general, but especially under these conditions, numerical flow simulations represent a powerful tool. In recent years, smoothed particle

hydrodynamics (SPH) has gained popularity due to the continuous improvement of computer hardware, especially regarding graphic processing units. In addition, only the CAD files are required, which is a significant advantage over Eulerian CFD codes where additional meshing is needed. However, the simulation of Pelton turbines with low specific speed presents additional difficulties owing to their distinct geometrical prerequisites and high velocity compared to the low discharge relation. The low flow rate at high jet velocities usually results in relatively small buckets compared to the size of the runner. This poses challenges not only for flow observation in experimental investigations but also for flow simulation. A minimal particle size would be required for the small bucket size and the thin jet diameter, both represented by particles. As the hardware on the GPU may overstep its capabilities, bigger particles must be used. However, tiny particles are needed to achieve both aims: a good representation of the runner surface and a sufficient resolution in the jet.

Additionally, the high velocity of the particles and the low discharge, leading to a small diameter of the jet, result in a fragile jet. So, modelling the binding forces and surface interaction in the bucket is far more critical than larger jet diameters with lower velocity and must be done carefully. In the Lagrangian approach, the particle-particle interaction and the particle-surface interaction are partly formed by particle size d_p, smoothing kernel length, interaction factor and particle shifting. To better understand the effects of the model behind these parameters, an open-source code was used for the present study, which allowed insight and validation of the mathematical formulations of the code.

This study uses the code DualSPHysics [1], an open-source software that utilises the smoothed particle hydrodynamics (SPH) method to enable the simulation of fluids and other continuous media within three-dimensional environments. With this code, a low specific speed Pelton turbine was analysed in detail based on the geometry of a one-nozzle Pelton turbine (in the following referenced as Prototype I). Particles represent the fluid, rotating, and static bodies. To save computing time, only the surface made of particles (the envelope) is used for the rotating runner and the housing. *Prototype I* has an n_q of 2.5 rpm and a head H of 350 m with a horizontal axis. One additional Pelton turbine with a different specific speed was investigated to evaluate the simulation setup with different geometrical conditions. The six-nozzle *Prototype II* had an n_q of 15.5 rpm ($n_{q,nozzle}$ = 6.3 rpm).

Prototype I has been tested in real size, and *Prototype II* has been tested in model size (scale factor as of 1:4.2, by applying similarity laws) in the Institute of Hydraulic Fluid machinery laboratory, which facilitated the verification of the simulation results.

2. PREPARATORY WORK

The simulation of Pelton turbines using SPH is becoming increasingly popular. Also, the SPH simulation with DualSPHysics [1] was already applied for this kind of turbine. Dominguez et al.'s work contains the mathematical model and code [2, 3]. Works by Furnes [4] conducted a comprehensive investigation into SPH on a Pelton turbine to determine if the approach of Pelton simulation with DualSPHysics is feasible for prediction and identified it as a promising tool. Ge et al. [5] compare mesh and particle-based approaches using the data from Vessaz; while he criticised the accuracy of the torque, he highlights the possibilities for preliminary screening. Further, he mentioned the benefits of droplet observation. Vessaz et al. [6, 7], who researched the finite volume particle method (FVPM) for Pelton turbines, described this method as satisfactory. Kumashiro et al. [8] used the particle-based software project “SPHEROS” to identify differences in torque compared to the mesh-based solution with ANSYS CFX, where the particle-based solver agreed with the experiment's trends. Furthermore, Alimirzazadeh et al. [9] examined the jet interference of six-jet Pelton turbines, utilising, for instance, SPHEROS as a meshless finite volume particle method (FVPM) for simulating fluid flows compared against ANSYS CFX, where the FVPM method was in agreement with the experiment and the jet interference good observable in the simulation.

Koukouvinis researched the flow in the injector of Pelton turbines [10] and improved conservation laws [11] for smoothed particle hydrodynamics. SPH development is still ongoing, as in the thesis of Garzon [12], who proposed a new ALE-WENO (Arbitrary Lagrangian Eulerian - Weighted Essentially Non-Oscillatory formulation) based on DualSPHysics for accurate free surface jets.

Arch and Mayr [13] note that the critical Weber number for droplets (or particles) is approximately 6.5. In this context, the particle Weber number under discussion is significantly higher; around ten times greater than this critical threshold. Additionally, the Weber number for the Pelton turbine aligns with this observation and is supported by the research conducted by Staubli and Hauser [14]. Their study of the Pelton turbine jet, with a similar Weber number, in Moccasin, California, revealed considerable droplet formation and mist, highlighting the instability of the jet's surface structure. “The higher the Weber number, the higher the degree of atomization.”, Grein et al. [15].

3. PARAMETERS

In preparation for the simulation, a parameter study focused on particle size and the smoothing and

shifting parameters. The initial parameters were derived from the so-called "DamBreak" example included in the DualSPHysics code package [16]. Then, an initial optimisation was evaluated by an analytically calculated torque from an impinging jet, with reference to existing literature (e.g. [10, 17]). For the optimisation process, a Nelder-Mead optimiser [18] was utilised to address the non-linear relationship between parameter changes and the resulting torque development [19, 20, 21] during the solving process [22].

After several iterations of jet impingement optimisation, the obtained parameters were applied to a single-bucket simulation. In this case, a full bucket was necessary, as using a half-model was not feasible due to the requirement to represent the edges as spheres (Asymmetry). Additionally, the shape of the jet was constrained by fundamental geometric forms, such as circles, making a half circle impossible within the current code. As a reference, the torque taken from the experiment was used as one benchmark for the simulation.

No numerical target value for correct fluid behaviour was available in the optimisation. Therefore, the parameter ranges for the optimisation were constantly fine-tuned manually to optimise torque and fluid behaviour simultaneously. For reference purposes, the simulation was, e.g., compared with Ruden's analytical analysis [23] concerning jet expansion. Experimental data from Schach [24] and other literature [25, 26, 27] were used to examine the jet's impact on a flat surface. Moreover, surface formation and wetting considerations were deemed important as they significantly influence the energy transfer (e.g., [28, 29]). Referencing from existing literature [30, 31, 32, 33, 34] was also applied to the bucket's fluid behaviour.

Subsequently, the derived parameters were utilised in a comprehensive runner simulation and compared against the measurement results from *Prototype I* and the literature [35, 36, 37]. Consequently, the simulation was analysed, leading to a re-run of the optimisation process at the jet impingement stage, whereas the results have been considered. The parameters acquired from this optimisation, particularly those related to shifting and smoothing, were also successfully used in the simulations for *Prototype II*.

3.1. PARTICLE SIZE

The size of the particle defines the resolution of the solid boundaries and the fluid. Moreover, numeric accuracy and computational performance are directly related to particle size and the boundary interaction between the fluid and the surface [4, 16, 2, 38]. Furthermore, DualSPHysics permits only identical particle sizes in a simulation.

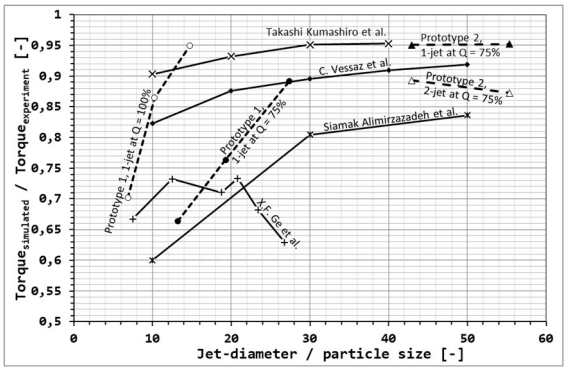

Figure 1. Different simulation results compared to literature values

Research [5, 9, 39, 40] indicates an interest in optimised particle size for particle simulation of Pelton turbines. Figure 1 shows the extracted and normalised data from the referenced researchers.

In addition, the separately simulated data is shown for comparison. On the one hand, the data generally indicates an improvement of the effective torque for higher jet diameter to particle size ratios (k_{d_p}). On the other hand, there is a decline in the achievable torque for different prototypes, similar to the findings of Ge et al. [5]. The assumption that the jet diameter to particle ratio, k_{d_p}, has an optimum or saturates at high values seems plausible, considering the Lagrangian formalisation [41, 42, 43].

$$k_{d_p} = \frac{d_{jet}}{d_p} \tag{1}$$

Considering the proposed ratio k_{d_p}, as expressed in Equation (1), a straightforward transition can be made with the jet velocity. As depicted in Equation (2), the jet diameter can be expressed in terms of discharge and head by reformulating the jet velocity and relating it to these variables, including the velocity coefficient k_c (e.g. K_{C_i} in Raabe [44]), which is a loss coefficient.

$$v_{jet} = k_c \cdot \sqrt{2 \cdot g \cdot H} = \frac{Q_{jet}}{A_{jet}} \tag{2}$$

This leads to the formula shown in Equation (3). The ratio k_{d_p} was taken from the literature (e.g., [8, 45]).

$$d_p = \frac{d_{jet}}{k_{d_p}} = \frac{2}{k_{d_p} \cdot (\pi \cdot k_c)^{\frac{1}{2}}} \cdot \frac{Q_{jet}^{\frac{1}{2}}}{(2 \cdot g \cdot H)^{\frac{1}{4}}} \tag{3}$$

The impact of the head and nozzle losses is smaller than the influence of the discharge. We simplify this further by collecting the jet velocity-related terms k_c and H, including the other constants, to a jet-velocity parameter k_{jv}, as seen in Equation (4).

$$k_{jv} = \frac{d_p \cdot k_{d_p}}{Q_{jet}^{\frac{1}{2}}} = \frac{2}{(\pi \cdot k_c)^{\frac{1}{2}}} \cdot \frac{1}{(2 \cdot g \cdot H)^{\frac{1}{4}}} \quad (4)$$

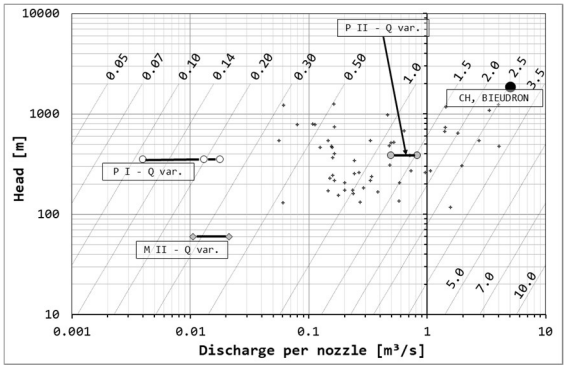

Figure 2. Lines of calculated constant particle size in mm for k_{dp} = 72, presented for discharge and head, g = 9.81 m/s² and k_c = 0.98, (+) are selected prototype units

This leads to the simplified form presented in Equation (5), where the terms are now divided into a kinetic energy factor (k_{jv}), discharge (Q), and numerical resolution (k_{d_p}).

$$d_p = \frac{d_{jet}}{k_{d_p}} = \frac{k_{jv}}{k_{d_p}} \cdot Q_{jet}^{\frac{1}{2}} \quad (5)$$

Figure 2 shows the simulated and other turbine data and the calculated lines for constant particle size with a k_{d_p} of 72, a gravitational acceleration g of 9.81 and a velocity coefficient k_c of 0.98. The value for k_{d_p} is constrained by the hardware and the solver. Selecting a large k_{d_p} value may cause the solver to raise an error due to the numerous potential particles in the system. For example, in DualSPHysics, the solver restricts the particle size by calculating a particle estimation before the simulation. Accordingly, after determining the appropriate particle size, it is essential to note that in DualSPHysics, there is no significant difference between using one or six nozzles in this memory safety measure. However, if the chosen particle size is too close to the limit, it could lead to the GPU running out of memory during the simulation. Consequently, a k_{d_p} value of 72 was employed for bucket simulations, whereas full simulations, including housing, utilised a k_{d_p} of 50, due to the memory of the GPU. Considering the trend presented in the literature and executed simulations, as depicted in Figure 1, it is suggested that an even higher k_{d_p} value of 72 and above could enhance the results.

Figure 3 depicts the particle size over the discharge per nozzle. In addition to the executed simulations, the calculated particle sizes, for example for Prototype I with $k_{d_p} = 100$ and the hardware limit, are included. The calculated particle size for *Prototype I*, where reducing the particle size would lead to an improvement, shows that the needed size is outside of the hardware possibilities. Further, the calculation of the particle size for the literature Pelton turbines shows that most of them would run below the actual hardware limit of an NVIDIA A6000 GPU.

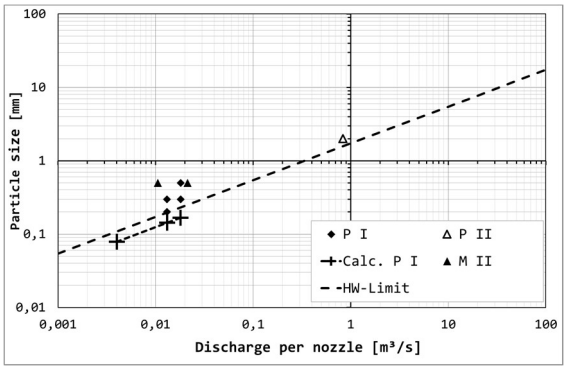

Figure 3. Comparison of applied particle size for various simulated Pelton turbines, calculated particle size (+, k_{dp} = 100) and the identified hardware limit for *Prototype I* (dashed line, k_{d_p} = 72)

When comparing the torque obtained from the simulation to the particle size used, a decline in torque corresponding to increasing particle sizes is observed. Figure 4 illustrates the deviation between simulated and experimental torque, correlating it with the relative increase in particle size compared to the calculation. For particles 5 to 9 times larger than the calculated size, the torque deviation is approximately 40% compared to the experiment. The smallest deviation corresponds to the calculated particle size with a k_{d_p} of 72.

The resulting trend, indicated by the dashed line in Figure 4 for *Prototype I*, suggests a tendency to saturate at both larger and smaller particle sizes. The simulation of *Prototype II* revealed a 5% torque deviation for the calculated particle size.

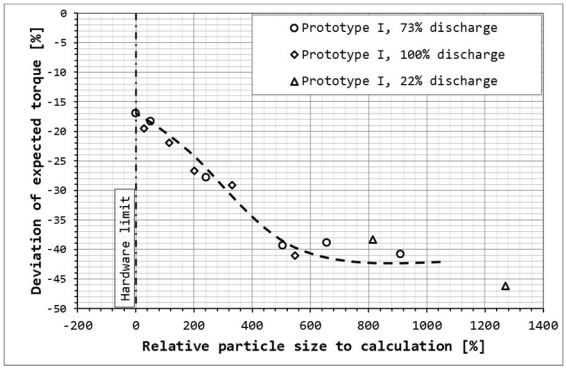

Figure 4. Torque deviation remains at approximately 40% even for particles 9 times larger than the calculated size, while the calculated particle size is the local minimum.

Further reducing the particle size should increase the possibilities of chaotic movement for the particles in the model, which leads to higher fluid-fluid interaction, ultimately reducing the energy transfer through friction. It is reasonable to assert that smaller particles result in only a limited improvement in energy transfer and are still below the expectations (a negative torque deviation far below 0) compared to the measurement for *Prototype I*.

4. SMOOTHING AND SHIFTING

The equation of state governs energy transfer within the Lagrangian framework of DualSPHysics [2] and similar SPH models. Therefore, key focus areas include the physical properties, particularly pressure and density. Taking a Pelton turbine as a reference, actual data should accurately represent these physical properties, which helps to define specific boundaries for parameters such as density, viscosity, and speed of sound. Furthermore, additional factors like solid-fluid binding coefficients [46] must be carefully chosen to maintain their linear characteristics. Model parameters, including kernel smoothing length and shifting [1], can be adjusted to improve fluid dynamics while preserving the integrity of the physical properties.

The kernel smoothing length is determined by the particle size and the smoothing coefficient $coef_h$ [2, 3]. This smoothing length indicates the distance to the considered neighbour particles for calculating the next time step, defined as the compact support area illustrated in Figure 5. For more details, Dominguez et al. [16, 2, 3] established the concepts of kernel and compact support within DualSPHysics.

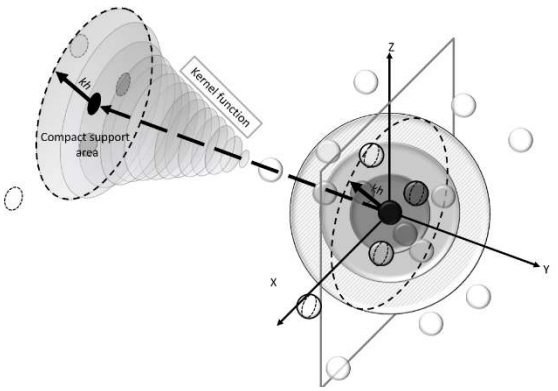

Figure 5. The influence of the kernel function depends on the smoothing length kh and the definition of the compact support area [33]. The right side represents the 3D particle space, while the left shows a conceptual 2D influence section with the kernel (interaction) function as an additional dimension.

An optimal solution would involve using an infinite smoothing length, effectively extending the compact support area to the entirety of the simulation domain, where every particle is considered for calculating a single particle for each time step. The constrained space and modelling predicated upon the ideal gas equation promote then the number of neighbouring elements. This leads to a transition toward regions of increased mass through the missing air particles and the damping of the kernel. With a small smoothing length, the compact support would approximate the particle size, allowing the particle to behave almost independently. Then, the interaction between two fluid particles or a fluid and boundary particle only occurs at a direct collision.

The following parameters in this parameter study are the “threshold to detect free surface”, referred to as the shifting parameter TFS and the coefficient for shifting computation [2]. Shifting defines the possible movement for the next time step, restricting the particle’s freedom.

Reduced freedom of the particles leads to rapid dispersion due to their high velocity. Therefore, a restriction should be imposed to ensure that the particles are forced to adhere to the initial flow. If the restriction is set too high, the particles face increased collisions due to the limited possibilities enforced by the flow and geometry. Thus, the shifting parameters should be chosen carefully to enable the particles to remain in the flow and follow the geometry without unnecessary collisions among the particles themselves.

A suitably selected shifting parameters and smoothing coefficient result in improved flow behaviour, enhancing the energy transfer between fluid and solid. Low parameter values facilitate higher freedom of movement. In comparison, higher values restrict potential motion, causing the fluid to adhere to the initial direction of the flow, consequently being more forced onto the solid when it gets redirected by the geometry of the bucket. This results in an unrealistic and strong deflection of the fluid on the bucket surface, which, due to the still restricted movement and high interaction radius of the particles, leads to the forming of a water bulk instead of a steady flow inside the bucket.

The coefficient for shifting computation was readily optimisable in jet impinging and remained unaffected by other parameters. The shifting coefficient TFS and the smoothing parameter $coef_h$ showed an interesting connection. This relationship suggests that there may be a significant link between them, which deserves further investigation. A simulation examining bucket interactions across various values of TFS and smoothing coefficients revealed that optimal torque occurs at a TFS of 0.3 and a smoothing coefficient of 0.8, as depicted in Figure 6. It is important to note that there is a marked decrease in torque at lower TFS values, while the smoothing coefficient exhibits a consistent decrease in both directions. Overall, the torque gradient for higher values of both parameters remains relatively flat. It is of high interest that the local optimum of the

torque is well-distinguished, which indicates a strong correlation for both parameters when applied to Pelton turbines.

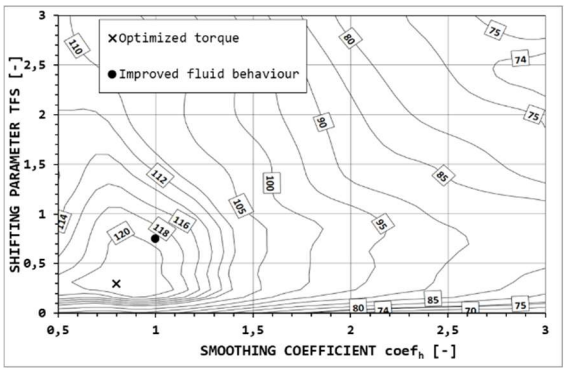

Figure 6. Torque variation in Nm over shifting parameters and smoothing coefficients of the bucket simulation for a fluid velocity of 82 m/s and a rotation speed of 1515 rpm

Further, in the optimum region, the fluid shows a substantial difference in the behaviour. Figure 7 illustrates the optimal torque on the left side, where the higher level of particle dispersion is evident. Moreover, the fluid behaviour is even worse for lower parameter values. By increasing the smoothing coefficient to one and adjusting the shifting parameter to 0.7, the fluid behaviour significantly improves, while the torque only decreases by around 1.5% (Figure 7, right side).

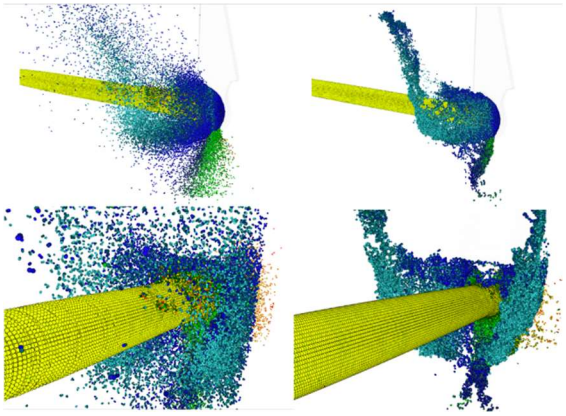

Figure 7. Single rotating bucket simulation with a fluid velocity of 82 m/s and rotation speed of 1515 rpm after torque optimisation (left) and after further manual correction of the shifting and the smoothing coefficient (right)

This divergence between the torque optimum and acceptable fluid movement indicates that energy transfer is better for more dispersive fluid behaviour. Nevertheless, fluid movement is essential for developing the Pelton turbine, particularly in the housing. Therefore, the optimisation must be revised, or an additional condition must be factored into the optimisation.

Table 1. Used parameters for DualSPHysics simulations of *Prototype I*, with highlighted parameters (bold) from the study

Parameter	Used value
Particle size d_p [mm]	**0.3**
Density ρ [kg/m³]	998.207
Dyn. Viscosity ν [Pa s]	8.93×10^{-7}
Speed of sound a [m/s]	1463.62
Boundary method	mDBC
Kernel	Wendland
Viscosity formulation	Laminar+SPS
Solid-fluid binding, ViscoBoundFactor	0.75
Smoothing coefficient $coef_h$	**1.102**
Shifting mode	Full
Threshold to detect free	**0.75**
Coefficient for shifting computation, ShiftCoef	-2.01
Minimum density valid [kg/m³]	900
Maximum density valid [kg/m³]	1100

After automated and manually corrected optimising *Prototype I*, a smoothing coefficient of 1.1 and a shifting parameter of 0.75 were identified. Further, the optimised $coef_h$ and TFS values yielded promising results for the fluid behaviour and the torque. In addition, the parameters used were successfully usable without adaptation for other simulations, such as *Prototypes II*.

Table 1 shows the set of used DualSPHysics parameters for the simulation of *Prototype I*.

5. JET DISTURBANCE

In the bucket work cycle, the bucket cuts through the jet before the filling begins. Observable in the experiment and CFD [47, 48], wetting occurs on the back side of the bucket, leading to a build-up of surface tension. The adhesive forces from the fluid-solid interaction create a pressure gradient called the Coanda effect [26, 27, 49], which pulls parts of the fluid towards the bucket's backside boundary layer.

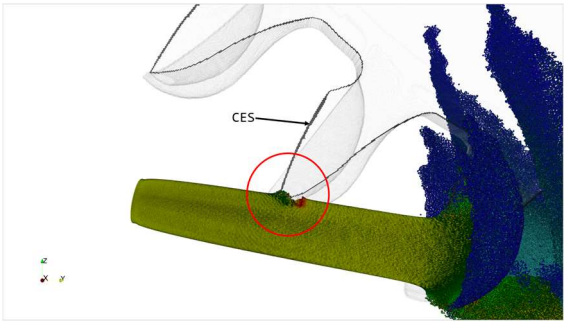

Figure 8. Initiation of jet disturbance (red) by entering the bucket at 7°, with highlighted cutting-edge section (CES)

In contrast, the fluid begins to move towards the bucket-runner connection. When the cohesive and

surface-forming forces reach their limit, the remaining jet after the bucket dissolves the connection.

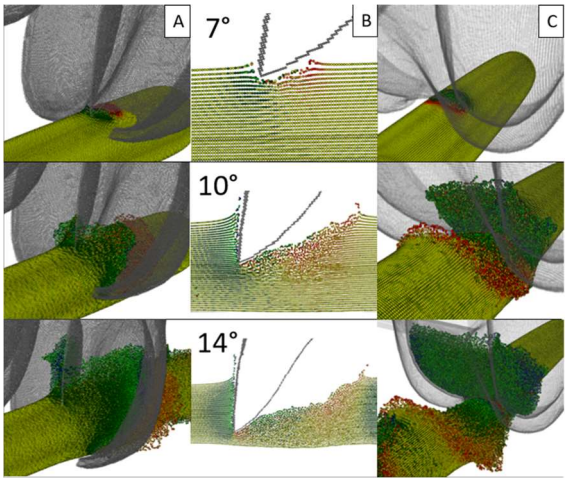

Figure 9. Jet disturbance for various positions over time with reduced (green), accelerated (red) and initial (yellow) particle speed in front view (A), cutting-edge section CES (B) and back view of the bucket

Compared with SPH, after the bucket enters the jet, a gap between the bucket's backside and the jet appears [5]. The needed surface terms are only indirectly considered through the ideal gas equation and the execution of the model [2, 49].

Furthermore, the volume's incompressibility (where density changes in the SPH to compensate for the fluid's incompressibility) leads to a push of the particles from the jet by the bucket, displacing the fluid inside the jet.

As a result, the jet becomes disturbed, and part of the particles accelerate. Figure 8 shows the initial disturbance caused by the bucket, while Figure 9 shows the development of the disturbance. The red marked area in Figure 8 is shown in Figure 9 for 7° in detail, including the highlighted cutting edge section (CES). When the bucket cuts into the jet, the particles of the jet are pushed by the rotating bucket. Hence, the particles change their trajectory, see Figure 10-B.

The pushed particles accelerate and generate additional momentum, which is transported in the jet direction. Furthermore, the accelerated particles in the direction of the jet displace the upstream particles, deforming the jet (see Figure 10-A) and creating a momentum wave within the jet (see Figure 9-C).

Similar to the observation of Ge et al. [5] or Guo et al. [50], this behaviour in the SPH is contrary to the physical expectation, where the surface tension and adhesive forces should create a pull towards the bucket's backside, along with a constriction of the jet.

Figure 10-C shows the development of the particle positioning, average velocity, and number of particles before (left), while bucket entrance (middle) and after (right).

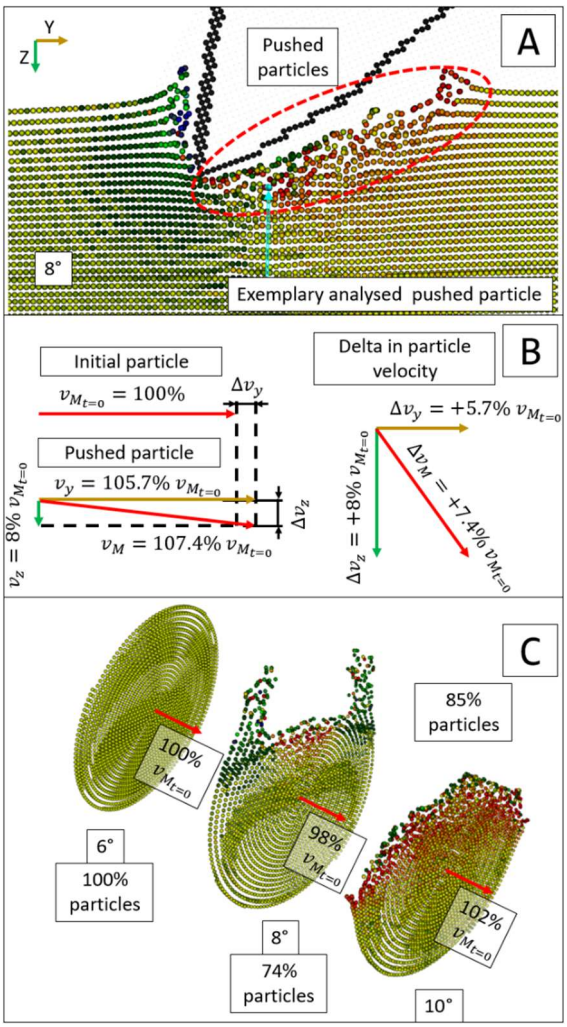

Figure 10. The relative development of velocity through the entrance of the bucket (A), accelerated particles (B), average velocity development (C) for 6° (before impact), 8° (impact) and 10° (after impact), including the number of particles in the sections

When the bucket cuts into the jet, some particles are removed through the bucket, some slow down by passing by the bucket, and others speed up (get pushed). The accelerated particles push against the particles in front of them. This interaction transfers some of their velocity to the front particles and increases the layer density. The first layers of particles that reach the bucket remain unchanged from the disturbance. Some accelerated particles in the following layers must move sideways past the main flow.

The particles that move sideways also impact the inner part of the bucket, causing further disturbances in the flow and resulting in energy loss.

The resulting disturbance is displayed in Figure 11, just before the impact and disturbance of the flow inside the bucket.

Furthermore, the disturbance can also be observed in the torque of a single bucket. Figure 12 illustrates the entrance of a single bucket into the jet for different particle sizes. For relatively large particles, specifically for *Prototype I* with $d_p = 2$ mm, the initial entrance is clearly visible at 2.25 ms (feature I).

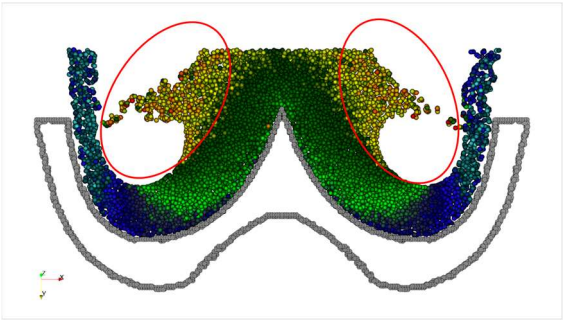

Figure 11. Jet disturbance in the bucket section

This negative torque nearly vanishes for reduced particle sizes. In addition, for a particle size of 2 mm, the initiated wave from the disturbance is distinctly distinguishable over the first milliseconds after bucket entrance (feature 1-4). Here, smaller particles exhibit no distinguishable wave but a weak promoted feature. Additionally, the difference between 0.5 mm and 0.7 mm particle sizes shows a shift of the characteristic peak from the wave impact around 3.25 (feature III) to 3.14 ms (feature II).

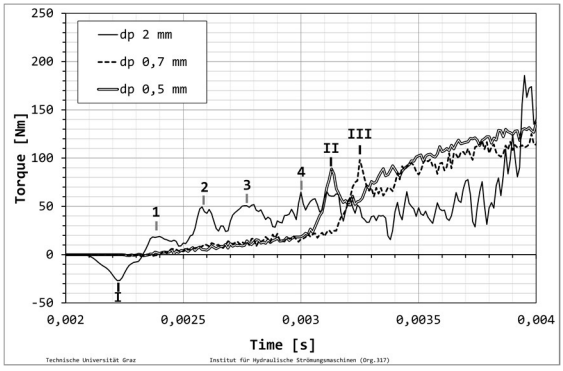

Figure 12: Change in torque through jet disturbance

6. SIMILARITY LAW

As dimensionless parameters for the similarity, φ and ψ are utilised. The discharge coefficient φ is defined with the bucket width B, discharge Q and runner speed n, shown in Equation (6) and normalised with the bucket number z for better comparison to the simulation. Further, the pressure coefficient ψ defined with head H,, runner diameter D and runner speed, depicted in Equation (7), is used.

Figure 13 illustrates discharge variations for *Prototype I* across heads of 350, 275, 200, and 100 m.

$$\varphi = \frac{8 \cdot Q}{B^3 \cdot \pi^2 \cdot z \cdot n} \tag{6}$$

$$\psi = \frac{2 \cdot g \cdot H}{D^2 \cdot \pi^2 \cdot n^2} \tag{7}$$

Additionally, a runner speed variation was conducted for constant discharge and head and a discharge variation for constant ψ. Similarly, several simulations were performed for each head at a constant discharge coefficient φ of 0.072.

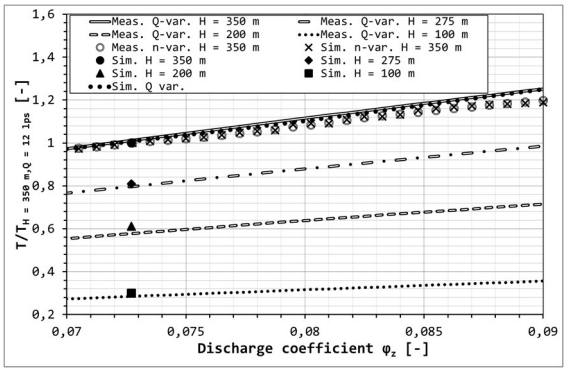

Figure 13 Relative torque of measurement compared to simulation

Furthermore, a simulation of the observed runner speed and discharge variations was conducted using identical values from the experiment. Subsequently, the torque from the measured and simulated operation points is normalised with the torque of the nominal operation point at $H = 350$ m. $n = 1515$ rpm at $\varphi = 0.072$.

In comparison, the relative torque change between the similar operating points for lower heads is nearly identical in both simulation and experiment. The discharge variation in the simulation shows a linear offset for higher discharges compared to the experiment, with a torque deviation below 1%. The variation in runner speed demonstrates a good match in the relative change in torque, which is almost identical to the relative change observed in the experiment.

CONCLUSION

This research examined the parameters in the software package DualSPHysics for particle size, smoothing coefficient, and shifting parameters for Pelton turbines, including the jet disturbance and similarity laws. An automated optimisation, including manual corrections and individual investigations, was conducted for the parameters.

As a result, the particle size was refined based on a simple correlation with discharge or jet diameter. The optimal particle size displayed a strong dependency on the jet diameter.

The shifting and smoothing parameters yielded a local optimum for torque, which does not align with acceptable fluid movement. A slight adaptation of the parameters allows a substantial improvement in fluid behaviour near the torque optimum.

In SPH, the occurring jet disturbance demonstrates the impact of the absent surface tension formulation within the model. Furthermore, the jet disturbance affects the torque, particularly for slender jets or jets with large particle sizes.

The investigation into the similarity law yielded favourable results when comparing operational points for identical geometries. However, an investigation between scaled geometries is still required.

The approach to support investigations with DualSPHysics is advantageous for low specific speed Pelton turbine development due to its limited effort and easy adaptation. Furthermore, the conservation of the similarity law can facilitate straightforward comparisons of changes between geometries and operational points.

ACKNOWLEDGEMENTS

This research has been performed at the Technical University of Graz, Institute of Hydraulic Fluid Machinery.

The product names referenced in this paper may be trademarks of their respective companies.

REFERENCES

[1] A. J. Crespo, J. M. Domínguez, B. D. Rogers, M. Gómez-Gesteira, S. Longshaw, R. Canelas, R. Vacondio, A. Barreiro and O. García-Feal, "DualSPHysics: Open-source parallel CFD solver based on Smoothed Particle Hydrodynamics (SPH)," *Computer Physics Communications,* vol. 187, pp. 204-216, 2 2015.

[2] J. M. Domínguez, G. Fourtakas, C. Altomare, R. B. Canelas, A. Tafuni, O. García-Feal, I. Martínez-Estévez, A. Mokos, R. Vacondio, A. J. Crespo, B. D. Rogers, P. K. Stansby and M. Gómez-Gesteira, "DualSPHysics: from fluid dynamics to multiphysics problems," *Computational Particle Mechanics,* 2021.

[3] J. M. A. Domínguez and G. Fourtakas, "Structure of the DualSPHysics code," in *DualSPHysics Users Workshop*, Manchester (United Kingdom), 2015.

[4] K. Furnes, "Flow in Pelton turbines," Norwegian University of Science and Technology, Department of Energy and Process Engineering, 2013.

[5] J. Sun, X. F. Ge and Y. Zheng, "SPH method used for characteristic predictions at Pelton turbine buckets: comparing with the mesh-based method," *Engineering Computations (Swansea, Wales),* vol. 40, no. 5, pp. 1245-1265, 7 2023.

[6] C. Vessaz, E. Jahanbakhsh and F. Avellan, "Flow simulation of a Pelton bucket using finite volume particle method," *IOP Conference Series: Earth and Environmental Science,* vol. 22, 2014.

[7] C. Vessaz, E. Jahanbakhsh and F. Avellan, "Flow simulation of jet deviation by rotating pelton buckets using finite volume particle method," *Journal of Fluids Engineering, Transactions of the ASME,* vol. 137, no. 7, 7 2015.

[8] T. Kumashiro, S. Alimirzazadeh, F. Avellan and K. Tani, "Application of particle-based numerical analysis to the practical design of Pelton turbine," *IOP Conference Series: Earth and Environmental Science,* vol. 774, no. 1, 6 2021.

[9] S. Alimirzazadeh, T. Kumashiro, S. Leguizamón, E. Jahanbakhsh, A. Maertens, C. Vessaz, K. Tani and F. Avellan, "GPU-accelerated numerical analysis of jet interference in a six-jet Pelton turbine using Finite Volume Particle Method," *Renewable Energy,* vol. 148, pp. 234-246, 4 2020.

[10] P. K. Koukouvinis, J. S. Anagnostopoulos and D. E. Papantonis, "Flow modelling in the injector of a Pelton turbine," in *4th international SPHERIC workshop*, Nantes, 2009.

[11] P. K. Koukouvinis, J. S. Anagnostopoulos and D. E. Papantonis, "An improved MUSCL treatment for the SPH-ALE method: Comparison with the standard SPH method for the jet impingement case," *International Journal for Numerical Methods in Fluids,* vol. 71, no. 9, pp. 1152-1177, 3 2013.

[12] R. A. Garzon, A NEW ALE-WENO FORMULATION OF SMOOTHED PARTICLE HYDRODYNAMICS (SPH) FOR THE ACCURATE SIMULATION OF FREE SURFACE JETS, Freie Universität Bozen, Faculty of Science and Technology, Sustainable Energy and Technologies, 2021.

[13] A. Arch and D. Mayr, "Prototype Measurements on casing flow and air entrainment into the tailwater of Pelton turbines," in *Measurement, 2. Jg., S. 1.*, LYON, 2009.

[14] T. Staubli and H. P. Hauser, "FLOW VISUALIZATION-A DIAGNOSIS TOOL FOR PELTON TURBINES," in *IGHEM*, Lucerne, 2004.

[15] H. Grein, D. Klicov and W. Wieser, "Efficiency scale effects in Pelton turbines," *Water Power & Dam Construction,* pp. 32-36, 1988.

[16] M. J. A. Domínguez, "DualSPHysics: Towards High Performance Computing using SPH technique," Universidad de Vigo, Enciromental Physics Laboratory, 2014.

[17] Z. Zhang, Freistrahlturbinen - Hydromechanik und Auslegung, Springer, 2009.

[18] J. A. Nelder and R. Mead, "A Simplex Method for Function Minimization," *The Computer Journal,* vol. 7, no. 4, pp. 308-313, 1 1965.

[19] C. H. Amon, A. M. Guzmán and B. Morel, "Lagrangian chaos, Eulerian chaos, and mixing enhancement in converging-diverging channel flows," *Physics of Fluids,* vol. 8, no. 5, pp. 1192-1206, 1996.

[20] D. Perrone, S. Stefania Scarsoglio, S. Luca Ridolfi and G. Boffetta, "Lagrangian dynamics in wall-bounded transitional and turbulent flows: Particle tracking and network-based analyses," 2024.

[21] L. P. Wang, M. R. Maxey, T. D. Burton and D. E. Stock, "Chaotic dynamics of particle dispersion in fluids," *Physics of Fluids A,* vol. 4, no. 8, pp. 1789-1804, 1992.

[22] M. M. Jalali and M. R. Jalali, "Curvilinear shallow water solver and Lagrangian particle tracking model for Chaotic advection," 2024.

[23] P. Ruden, "Turbulente Ausbreitungsvorgänge im Freistrahl," *Die Naturwissenschaften, Springer Verlag,* vol. 21, no. 23, pp. 375-378, 1933.

[24] W. Schach, "Umlenkung eines kreisförmigen Flüssigkeitsstrahles an einer ebenen Platte senkrecht zur Strömungsrichtung," *Ingenieur-Archiv, Springer Verlag,* vol. VI, pp. 51-59, 1934.

[25] MABROUKI T., Raissi K. and Cornier A., "Numerical simulation and experimental study of the interaction between a pure high-velocity waterjet and targets: contribution to investigate the decoating process," *ELSEVIER WEAR,* no. 239, pp. 260-273, 1 2000.

[26] F. Chen and P. E. Smith, "Simulated surface tensions of common water models," *Journal of Chemical Physics,* vol. 126, no. 22, 2007.

[27] M. Miozzi, F. Lalli and G. P. Romano, "Experimental investigation of a free-surface turbulent jet with Coanda effect," *Experiments in Fluids,* vol. 49, no. 1, pp. 341-353, 7 2010.

[28] P. Jungwirth and D. J. Tobias, "Specific ion effects at the air/water interface," *Chemical Reviews,* vol. 106, no. 4, pp. 1259-1281, 4 2006.

[29] S. Chempath and L. R. Pratt, "Distribution of binding energies of a water molecule in the water liquid-vapor interface," *Journal of Physical Chemistry B,* vol. 113, no. 13, pp. 4147-4151, 4 2009.

[30] Y. NAKANISHI, T. FUJII and S. KAWAGUCHI, "Numerical and Experimental Investigations of the Flow in a Stationary Pelton Bucket," *Journal of Fluid Science and Technology,* vol. 4, no. 3, pp. 490-499, 2009.

[31] C. Bauer, Visualisierung von Strömungen im Becher einer Peltonturbin, Technische Universität Wien, Institut für Energietechnik und Thermodynamik, Forschungsbereich Strömungsmaschinen, 2011.

[32] J.-C. Marongiu, F. Leboeuf, J. Caro, E. Parkinson and E. Parkinson Free, "Free surface flows simulations in Pelton turbines using an hybrid SPH-ALE method," *Journal of Hydraulic Research,* vol. 48, pp. 40-49, 2010.

[33] F. Beck and P. Eberhard, "Predicting abrasive wear with coupled Lagrangian methods," *Computational Particle Mechanics,* vol. 2, no. 1, pp. 51-62, 5 2015.

[34] A. Rossetti, G. Pavesi, G. Cavazzini, A. Santolin and G. Ardizzon, "Influence of the bucket geometry on the Pelton performance," *Proceedings of the Institution of Mechanical Engineers, Part A: Journal of Power and Energy,* vol. 228, no. 1, pp. 33-45, 2014.

[35] T. Kubota, "Observation d'interférence de jets dans une turbine pelton à 6 injecteurs," *Journal of Hydraulic Research,* vol. 27, no. 6, pp. 753-767, 1989.

[36] F. Beck and P. Eberhard, "Comparison of wear models using a Lagrangian approach," in *IV International Conference on Particle-based Methods–Fundamentals and Applications PARTICLES2015*, 2015.

[37] J.-C. Marongui, M. Rentschler and E. Parkinson, "Study of flow patterns in hydraulic turbines with SPH-Ale," Hydrolink, 2015.

[38] A. Židonis and G. A. Aggidis, "State of the art in numerical modelling of Pelton turbines," *Renewable and Sustainable Energy Reviews,* vol. 45, pp. 135-144, 2015.

[39] C. Vessaz, L. Andolfatto, F. Avellan and C. Tournier, Toward design optimization of a Pelton turbine runner, vol. 55, Springer Verlag, 2017, pp. 37-51.

[40] T. Kumashiro, S. Alimirzazadeh, A. Maertens, E. Jahanbakhsh, S. Leguizamón, F. Avellan and K. Tani, "Numerical investigation of the jet velocity profile and its influence on the Pelton turbine performance," *IOP*

Conference Series: Earth and Environmental Science, vol. 240, no. 7, 3 2019.

[41] A. Frangioni, "About Lagrangian Methods in Integer Optimization," *Annals of Operations Research,* vol. 139, pp. 163-193, 2005.

[42] X. Q. Yang, X. X. Huang and S. J. Optim, "A nonlinear Lagrangian approach to constrained optimization problems," *SIAM journal of optimisation,* vol. 11, no. 4, pp. 1119-1144, 2001.

[43] S. Sabach and M. Teboulle, "Lagrangian Methods for Composite Optimization," 2019.

[44] J. Raabe, Hydro power. The design, use, and function of hydromechanical, hydraulic and electrical equipment, VDI-Verlag, 1985.

[45] C. VESSAZ, "Finite Particle Flow Simulation of Free Jet Deviation by Rotating Pelton Buckets," 2015.

[46] D. team, "XML guide for DualSPHysics," DualSPHysics, 2022.

[47] A. Perrig, "Hydrodynamics of the free surface flow in Pelton turbine buckets," EPFL, Lausanne, 2007.

[48] M. Choi, Y. J. Jung and Y. Shin, Unsteady flow simulations of Pelton turbine at different rotational speeds, vol. 7, Hindawi Publishing Corporation, 2015.

[49] A. ŽIDONIS, OPTIMISATION AND EFFICIENCY IMPROVEMENT OF PELTON HYDRO TURBINE USING COMPUTATIONAL FLUID DYNAMICS AND EXPERIMENTAL TESTING, Lancaster University, 2015.

[50] B. Guo, Y. Xiao, A. K. Rai, Q. Liang and J. Liu, "Analysis of the air-water-sediment flow behavior in Pelton buckets using a Eulerian-Lagrangian approach," *Energy,* vol. 218, 3 2021.